energies

MDPI

Article

A Quantitative Risk-Averse Model for Optimal Management of Multi-Source Standalone Microgrid with Demand Response and Pumped Hydro Storage

Yongqi Zhao † and Jiajia Chen *,†

School of Electrical and Electronic Engineering, Shandong University of Technology, Zibo 255049, China; zyq@sdut.edu.cn

* Correspondence: jjchen@sdut.edu.cn

† Current address: 266 Xincun West Road, Zhangdian District, Zibo 255049, China.

Abstract: High renewable energy integrated standalone microgrid requires greater ramping capabilities from other dispatchable resources to compensate for effects of the intermittent and variability of the renewable energy available in the system. To address this, a wind-solar-thermal-hydro-coupled multi-source standalone microgrid (WSTHcMSSM) considering demand response and pumped hydro storage is proposed to maximize the operating profit and get the optimal solution of the multi-source generation system by taking advantage of multi-resource complementarity. In WSTHcMSSM, we present a conditional value-at-credibility (CVaC)-based quantitative risk-averse model for uncertain wind and solar power by thoroughly examining the randomness and fuzziness characteristics. Additionally, the most severe issues caused by wind and solar power fluctuation happen during the peak load, and this paper proposes a load partitioning method to get the time-of-use (TOU) in demand response for peak load shaving. A case study is conducted for the validation of the proposed method. It is found from the study case that the CVaC can well evaluate the uncertainty in WSTHcMSSM with wind and solar integration. Additionally, the WSTHcMSSM can efficiently explore the potential flexibility in multi-source complementarity for promoting the penetration of renewable energy.

Keywords: conditional value-at-credibility; demand response; pumped hydro storage; risk evaluation; standalone microgrid

Citation: Zhao, Y.; Chen, J. A Quantitative Risk-Averse Model for Optimal Management of Multi-Source Standalone Microgrid with Demand Response and Pumped Hydro Storage. *Energies* **2021**, *14*, 2692. https://doi.org/10.3390/en14092692

Academic Editor: Gianfranco Chicco

Received: 16 March 2021
Accepted: 28 April 2021
Published: 7 May 2021

1. Introduction

The increasing issues of the environment and climate change are becoming increasingly vital constraints on power industry development. In the past few years, interests in the use of renewable energy have been growing steadily [1,2]. However, the inherent intermittency and variability of renewable resource (e.g., wind and solar) increase the fluctuation of net load significantly and require additional flexibility resources to smooth the load curve [3,4]. Besides, in cases where wind and solar generation are more than load minus must-run generation, the excess of wind and solar power has to be curtailed to ensure the power balance between the demand side and supply side. Thereby, it poses significant challenges to the safe and economic operation of standalone microgrid with a high penetration level of wind and solar power. Both battery storage and hydro storage are a topic of great importance for addressing the uncertain renewable energy. However, the authors in [5] stated that hydro storage is more cost-competitive than battery storage, and presents practical potential and technically feasible opportunities for power supply in remote areas. Thus, coordinating the traditional controllable hydropower with the uncontrollable wind and solar power to form a hybrid multi-source microgrid is a promising solution for promoting renewable energy penetration [6,7].

There have been many works in the literature to investigate the coordinated operation of wind-solar-thermal-hydro (WSTH) from various aspects. For instance, Reference [8]

proposed a complementary operation of WSTH system to address the problem of renewable energy curtailment, considering minimizing the fluctuation of thermal output and maximizing the penetration of renewable energy. Reference [9] developed a new strategy for the day-ahead operation of the WSTH system with storage, which aims to provide the "best-fit" scheduling by minimizing day-ahead and real-time operation costs. The authors in [10] explored the principle of wind-hydro compensation, and the principle was also quantitatively analyzed in a power grid. In [11], a multi-time-scale dispatching mechanism for WSTH and battery was proposed to handle renewable energy fluctuations. Note that unlike conventional controllable units, the outputs of wind power and solar power are highly uncertain and unpredictable. Even the best commercially available methods applied in wind/solar precasting are with the 15–20% error [12]. It should be noted that even with 10–15% error, it may result in great uncertainties for the balance of supply and demand, which affects the optimal power system operation [13–15]. For example, Reference [16] studied the output shortage, spilled water, and power curtailment risk in WSTH system to enhance resource utilization efficiency. In [17], the authors investigated the effectiveness of locational marginal pricing in WSTH to reduce the wind power curtailment. In [18], a model predictive control method was developed to address the frequency issue with considering the intermittent generation. Hence, the coordinated operation strategy of WSTH system is still needed, especially in a scenario of large scale penetration of uncertain renewable energy.

The risk management methods for uncertain wind and solar power have been studied in many papers. From existing literature, the stochastic optimization method has been successfully used in stochastic microgrid scheduling for addressing various uncertainties [19–21]. This method is inspired by portfolio optimization, and aims to study how to get the optimal penetration level of uncertain renewable energy. In [22], authors proposed to use the mean-variance (MV) model to deal with the wind power integrated stochastic power flow problem. Note that the MV is based on the assumption that the utility distribution functions are quadratic, or the return of each asset is with a norm distribution [23]. The study carried out by Chen et al. [24] pointed out that the MV is not suitable to be employed for addressing uncertain wind power due to the fact that the returns brought by wind power are not symmetrically distributed around the mean. Noting that using variance as the risk measure may sacrifice the higher return in stochastic optimization [25], semi-variance was employed in [26] in an uncertain power system environment, which tries to get the undesirable deviation of uncertain wind power. Comparison results illustrated that semi-variance is more convincing and reliable for stochastic power system scheduling under risk aversion [26,27]. However, the variance and semi-variance rely on the distribution of cost expectation, and they are not sufficient to describe the uncertain risk when the cost expectation does not follow normal distribution [28]. In addition, the authors in [24] asserted that in non-normal cost expectation, the higher moments should be considered in decision making of power system optimization.

All aforementioned risk evaluation methods were formulated based on the probability theory by characterizing the uncertainty as a random variable. Besides, stochastic optimization relies on the repeated samplings, and is thought of as occupying much time. Some researchers in the literature stated that many fuzzy characteristics exist commonly in stochastic power system operation, so that the returns brought by intermittent and variable renewable energy contain other aspects of uncertainty, such as ambiguity and vagueness [13,29]. Abdul-Rahman and Shahidehpour [30] stated that the uncertainty of bus loads can be addressed using a fuzzy set based optimization model. Subsequently, in renewable energy integrated optimization problems, the uncertainty can also be addressed by fuzzy optimization [31–33]. However, the study carried out by Simoneli [34] indicated that taking the variance as a risk index is less convincing than entropy in asset allocation. For example, Armando et al. employed entropy to evaluate the loss of load risk in generating systems [35] and overloads risk in transmission equipment [36]. However, entropy evaluates the uncertainty of cost expectation with low and high extreme situations, and it

will inevitably sacrifice the higher assets brought by renewable energy and limit its penetration level. Besides, in the situation of high energy consumption, the available dispatchable resources to address the fluctuation are already used, and a sudden reduction of wind or solar power output can have critical consequences on the system reliability [37,38]. In view of the above discussion, the main contributions of this paper can be summarized as below:

- This paper presents a WSTH-coupled multi-source standalone microgrid (WSTHcMSSM) considering pumped hydro storage and demand response (DR) to mitigate the challenge of supply and demand imbalance, resulting in the effect of promoting wind and solar power consumption.
- A conditional value-at-credibility (CVaC)-based quantitative risk-averse model is first developed to address the uncertainty of wind and solar power in WSTHcMSSM system, making the system reach a trade-off option.
- In consideration that the most severe issues caused by wind and solar power fluctuation happen during the peak load, this paper proposes a load partitioning method to determine the time-of-use (TOU) price in DR to explore the potential flexibility of WSTHcMSSM microgrid scheduling.

The rest of the paper is organized as follows. Section 2 models the energy systems of WSTHcMSSM. Section 3 formulates the CVaC-based risk evaluation for WSTHcMSSM. Section 4 gives the numerical studies. Finally, a conclusion and interesting future work are drawn in Section 5.

2. System Modeling

Figure 1 depicts an overview of the studied WSTHcMSSM. The multi-source standalone microgrid includes wind power and solar power as uncertain resources, micro-turbine and pumped hydro storage as the dispatchable resources, demand response as the flexible improvement technique, and some smart users. The main goal of the smart microgrid center is to maximize the operation profit by scheduling different kinds of generation sources whilst satisfying all network constraints. To this end, the information, such as forecasted values of wind and solar power, time-of-use price, and initial load demand, is firstly collected by the smart microgrid center. Then, based on the model of existing equipment and their operation constraints, the optimal dispatch solution is taken by the smart microgrid center. The dispatch solution includes optimal outputs of wind, solar, pumped hydro storage and micro-turbine, considering the DR of smart users. We investigate the WSTHcMSSM for a scheduling horizon in a typical working day divided into $T = 24$ equal times slots. The mathematical description of equipment and its physical constraints in WSTHcMSSM is given below.

2.1. Micro-Turbine Generation Model

Note that considering the zero incremental cost of renewable energy and hydro energy [39], in WSTHcMSSM schedule framework, the operation cost refers to the cost of micro-turbine for electric power generation and start-up cost shown by:

$$G = \sum_{t=1}^{T} \left[\sum_{g=1}^{N_{\mathrm{MT}}} u_{\mathrm{MT}}(g,t) \Big(F_g\big(P_{\mathrm{MT}}(g,t)\big) + s_g\big(u_{\mathrm{MT}}(g,t)\big) \Big) \right] \tag{1}$$

where

$$F_g\big(P_{\mathrm{MT}}(g,t)\big) = a_{1g}\big(P_{\mathrm{MT}}(g,t)\big)^2 + a_{2g}P_{\mathrm{MT}}(g,t) + a_{3g},$$

$$s_g\big(u_{\mathrm{MT}}(g,t)\big) = K_g\Big(1 - s_g\big(u_{\mathrm{MT}}(g,t-1)\big)\Big).$$

N_{MT} is the number of micro-turbines. The binary variable $u_{\mathrm{MT}}(g,t) \in \{0,1\}$ is the indicator of the gth micro-turbine state at time t, where $u_{\mathrm{MT}}(g,t) = 1$ denotes that the gth micro-turbine is in the state ON during time t, while $u_{\mathrm{MT}}(g,t) = 0$ denotes that the gth micro-turbine is in the state OFF during time t. $P_{\mathrm{MT}}(g,t)$ denotes the micro-turbine

output with respect to cost coefficients a_{1g}, a_{2g}, a_{3g} of the gth turbine at time t. $s_g(u_{\mathrm{MT}}(g,t))$ represents the start-up cost, where K_g is a start-up parameter.

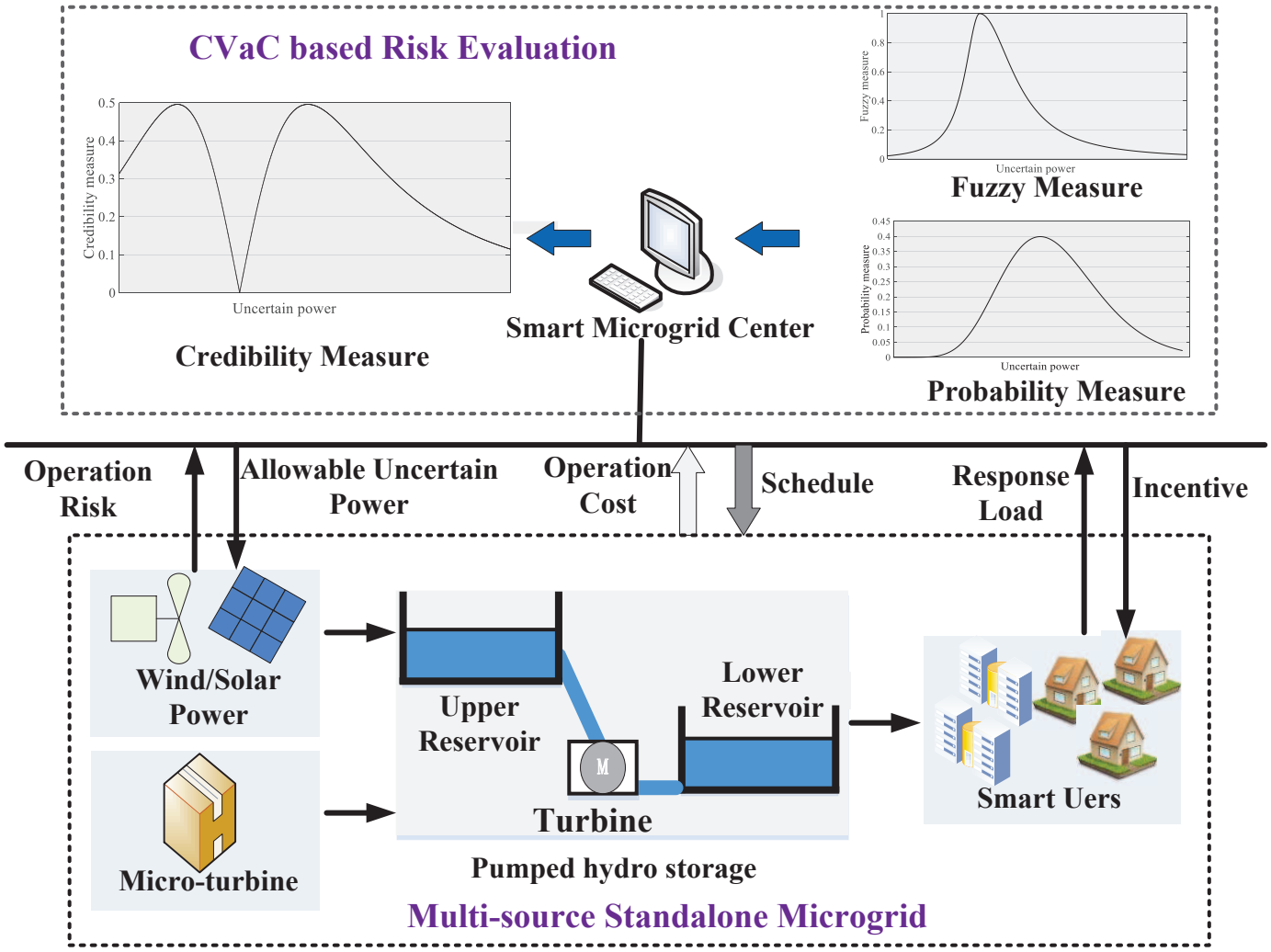

Figure 1. Configuration of the WSTHcMSSM.

The micro-turbine operations are constrained as ($\forall t \in T, g \in N_{\mathrm{MT}}$):

$$P_{\mathrm{MT}}^{\min}(g) \le P_{\mathrm{MT}}(g,t) \le P_{\mathrm{MT}}^{\max}(g) \tag{2a}$$

$$P_{\mathrm{MT}}(g,t) - P_{\mathrm{MT}}(g,t-1) \le u_{\mathrm{MT}}(g,t-1)\mathrm{RU}_{\mathrm{MT}}(g) + \left(1 - u_{\mathrm{MT}}(g,t-1)\right)P_{\mathrm{MT}}^{\max}(g) \tag{2b}$$

$$P_{\mathrm{MT}}(g,t-1) - P_{\mathrm{MT}}(g,t) \le u_{\mathrm{MT}}(g,t)\mathrm{RD}_{\mathrm{MT}}(g,t) + \left(1 - u_{\mathrm{MT}}(g,t)\right)P_{\mathrm{MT}}^{\min}(g) \tag{2c}$$

$$T_{\mathrm{on}}(g) \ge T_{\mathrm{up}}(g) \tag{2d}$$

$$T_{\mathrm{off}}(g) \ge T_{\mathrm{down}}(g) \tag{2e}$$

where (2a) represents generation limits, and $P_{\mathrm{MT}}^{\min}(g)$ and $P_{\mathrm{MT}}^{\max}(g)$ are, respectively, the lower and upper generation boundaries of the gth micro-turbine. Equations (2b) and (2c) denote ramp constraints, where $\mathrm{RU}_{\mathrm{MT}}(g)$ and $\mathrm{RD}_{\mathrm{MT}}(g)$ are, respectively, the ramp-up and ramp-down rate of the gth micro-turbine. Equations (2d) and (2e) model the minimum up and down time constraints, which ensure the running time $T_{\mathrm{on}}(g)$ of the gth turbine is equal to or greater than the minimum micro-turbine uptime $T_{\mathrm{up}}(g)$, and the down time $T_{\mathrm{off}}(g)$ is equal to or greater than the minimum micro-turbine downtime $T_{\mathrm{down}}(g)$.

2.2. Pumped Hydro Storage Generation Model

At time t, the water-to-power function of the hth hydro turbine $P_{\mathrm{H}}(h,t)$ can be modeled by a quadratic polynomial of reservoir volume $Q(h,t)$ and water discharge $V(h,t)$:

$$P_{\mathrm{H}}(h,t) = b_{1h}V(h,t)^2 + b_{2h}Q(h,t)^2 + b_{3h}V(h,t)Q(h,t) + b_{4h}V(h,t) + b_{5h}Q(h,t) + b_{6h} \quad (3)$$

where $b_{1h}, b_{2h}, b_{3h}, b_{4h}, b_{5h}$, and b_{6h} are generation coefficients of hydro turbine h.

The pumped hydro storage satisfies the hydraulic continuity constraints [40], i.e., the water discharge $V(h,t)$ is constrained by:

$$V(h,t) = I(h,t) + V(h,t-1) - S(h,t) - Q(h,t) + \sum_{h' \in R_u(h)} \left(Q(h', t-\tau_{h'h}) + S(h', t-\tau_{h'h})\right) \quad (4a)$$

$$V^{\min}(h) \le V(h,t) \le V^{\max}(h) \quad (4b)$$

$$V^{\mathrm{I}}(h) = V(h,0), V^{\mathrm{F}}(h) = V(h,T) \quad (4c)$$

$$Q^{\min}(j) \le Q(j,t) \le Q^{\max}(j) \quad (4d)$$

$$P_{\mathrm{H}}^{\min}(h) \le P_{\mathrm{H}}(h,t) \le P_{\mathrm{H}}^{\max}(h) \quad (4e)$$

where Equation (4a) relates the water discharge balance constraint, $I(h,t)$ denotes the external inflow to the hth reservoir at time t, $S(h,t)$ represents the spillage discharge rate of reservoir h at time t, and $\tau_{h'h}$ is the water transport delay from the h'th to the hth reservoir. Equation (4b) indicates that the water discharge is limited by the minimum and maximum storage value. $V^{\min}(h)$ and $V^{\max}(h)$ are, respectively, the lower and upper volume limits of reservoir h. Equation (4c) takes into account the initial and final reservoir storage volume constraints. $V(h,0)$ and $V(h,T)$ represent storage volumes of the hth reservoir at time 0 and T, respectively; as for $V^{\mathrm{I}}(h)$ and $V^{\mathrm{F}}(h)$, they are, respectively, the hth reservoir's initial and final volumes. Equation (4d) represents the water discharge limitation constraint, where $Q^{\min}(h)$ and $Q^{\max}(h)$ are, respectively, the minimum and maximum boundaries of reservoir h. In addition, the hydro turbine should also satisfy power output limits shown in (4e), where $P_{\mathrm{H}}^{\min}(h)$ and $P_{\mathrm{H}}^{\max}(h)$ are, respectively, the minimum and maximum generation limits of turbine h.

2.3. Distribution Characteristic of Wind and Solar

As stated in [22,24,26], in short-term power system schedule, the errors of wind and solar can be simulated by Gaussian distribution based on the central limit theorem [41]. At time t, denote $P_{\mathrm{W}}(t)$ and $P_{\mathrm{S}}(t)$ as actual outputs of wind and solar, respectively, then distribution characteristics of wind power and solar power can be expressed by forecasting outputs and forecasting errors:

$$P_{\mathrm{W}}(t) \sim \mu_{\mathrm{W}}(t) + N(0, \sigma_{\mathrm{W}}(t)) \quad (5)$$

$$P_{\mathrm{S}}(t) \sim \mu_{\mathrm{S}}(t) + N(0, \sigma_{\mathrm{S}}(t)) \quad (6)$$

where $\mu_{\mathrm{W}}(t)$ and $\mu_{\mathrm{S}}(t)$ are, respectively, forecasting values of wind and solar power during time t, and $\sigma_{\mathrm{W}}(t)$ and $\sigma_{\mathrm{S}}(t)$ denote forecasting standard deviations associated with wind and solar at time t, respectively.

Considering a 95% confidence level, the outputs of wind and solar power satisfies:

$$\mu_{\mathrm{W}}(t) - 1.96\sigma_{\mathrm{W}}(t) \le P_{\mathrm{W}}(t) \le \mu_{\mathrm{W}}(t) + 1.96\sigma_{\mathrm{W}}(t) \quad (7a)$$

$$\mu_{\mathrm{S}}(t) - 1.96\sigma_{\mathrm{S}}(t) \le P_{\mathrm{S}}(t) \le \mu_{\mathrm{S}}(t) + 1.96\sigma_{\mathrm{S}}(t) \quad (7b)$$

where $P_{\mathrm{W}}^{\min}$ and $P_{\mathrm{W}}^{\max}$ are, respectively, the minimum and maximum outputs of wind turbine w at time t, and $P_{\mathrm{S}}^{\min}$ and $P_{\mathrm{S}}^{\max}$ are, respectively, the minimum and maximum outputs of solar station s at time t.

3. CVaC-Based Risk Evaluation for WSTHcMSSM

Given the system load demand, hydraulic continuity limits, water discharge limits, reservoir storage volume limits, unit generation limits, and available wind and solar power at a specified time horizon, this paper presents a conditional value-at-credibility (CVaC) model to quantitatively evaluate the uncertain risk associated with wind and solar forecasting error, and optimally dispatch of micro-turbine, wind turbine, solar station, and hydro source in WSTHcMSSM system, which amounts to taking the advantage of multi-source complementarity. To this end, the optimization objective and operation constraints of the CVaC-based WSTHcMSSM with DR and pumped hydro storage are given as follows:

$$\max \sum_{t=1}^{T} \rho(t) \left(\nu(P_{\mathrm{W}}(t)) P_{\mathrm{W}}(t) + \nu(P_{\mathrm{S}}(t)) P_{\mathrm{S}}(t) + \sum_{g}^{N_{\mathrm{MT}}} u_{\mathrm{MT}}(g,t) P_{\mathrm{MT}}(g,t) + \sum_{h}^{N_{\mathrm{H}}} P_{\mathrm{H}}(h,t) \right) - G \tag{8a}$$

$$\text{s.t.} P_{\mathrm{W}}(t) + P_{\mathrm{S}}(t) + \sum_{g}^{N_{\mathrm{MT}}} u_{\mathrm{MT}}(g,t) P_{\mathrm{MT}}(g,t) + \sum_{h}^{N_{\mathrm{H}}} P_{\mathrm{H}}(h,t) = P_{\mathrm{D}}(t) \tag{8b}$$

$$(2) - (7) \tag{8c}$$

$$\rho(t) = \begin{cases} \rho_0 - \Delta\rho(t), t \in G_1 \\ \rho_0, t \in G_2 \\ \rho_0 + \Delta\rho(t), t \in G_3 \\ \Delta\rho_{\min}(t) \le \Delta\rho(t) \le \Delta\rho_{\max}(t) \end{cases} \tag{8d}$$

where (8a) represents the operation profit of WSTHcMSSM by selling power to end users, $\rho_0(t)$ denotes the fixed price at time t, $\rho(t)$ represents the time-of-use (TOU) price at time t, N_{H} denotes the number of hydro turbines, $\nu(\cdot)$ denotes risk measures with respect to wind or solar power and it will be given in the following subsection. In view of this, the objective function defined in this paper is the profit of WSTHcMSSM. (8c) represents the system power balance constraint. (8d) represents the TOU price constraints, where G_1, G_2 and G_3 are, respectively, load sets of valley period, flat period and peak period, and $\Delta\rho_{\min}(t) = 0.1\rho_0$ and $\Delta\rho_{\max}(t) = \rho_0$ are, respectively, the lower and upper values of price deviation $\Delta\rho(t)$ during time t.

3.1. CVaC for Uncertain Wind and Solar Power

In this subsection, to facilitate the analysis, we take one wind turbine and one solar station for example. At time t, the joint probability density function of wind and solar power $\phi(x(t))$, where $x(t) = [P_{\mathrm{W}}(t), P_{\mathrm{S}}(t)]^T$, can be expressed by:

$$\phi(x(t)) = \frac{1}{\sqrt{(2\pi)^2 |B(t)|}} e^{-\frac{1}{2}(x(t)-\mu(t))^T B(t)^{-1} (x(t)-\mu(t))} \tag{9}$$

where $B(t)$ denotes the covariance matrix, and $\mu(t) = [\mu_{\mathrm{W}}(t), \mu_{\mathrm{S}}(t)]^T$. Then, the expected values $Q_{\mathrm{W}}(t)^-$ and $Q_{\mathrm{S}}(t)^-$ associated with the materialized outputs $P_{\mathrm{W}}(t)$ and $P_{\mathrm{S}}(t)$ not exceeding the forecasting values $\mu_{\mathrm{W}}(t)$ and $\mu_{\mathrm{S}}(t)$ can be expressed by Equations (10) and (11), respectively.

$$Q_{\mathrm{W}}(t)^- = \int_{\mu_{\mathrm{W}}(t) - 1.96\sigma_{\mathrm{W}}(t)}^{\mu_{\mathrm{W}}(t)} (\mu_{\mathrm{W}}(t) - y) \phi(y) dy \tag{10}$$

$$Q_{\mathrm{S}}(t)^- = \int_{\mu_{\mathrm{S}}(t) - 1.96\sigma_{\mathrm{S}}(t)}^{\mu_{\mathrm{S}}(t)} (\mu_{\mathrm{S}}(t) - z) \phi(z) dz \tag{11}$$

Similarly, the expected values $Q_W(t)^+$ and $Q_S(t)^+$ associated with the materialized outputs exceeding the forecasting values can be expressed by Equations (12) and (13), respectively.

$$Q_W(t)^+ = \int_{\mu_W(t)}^{\mu_W(t)+1.96\sigma_W(t)} (y - \mu_W(t))\phi(y)dy \tag{12}$$

$$Q_S(t)^+ = \int_{\mu_S(t)}^{\mu_S(t)+1.96\sigma_S(t)} (z - \mu_S(t))\phi(z)dz \tag{13}$$

Besides the random characteristics, the outputs of wind and solar power also have fuzzy characteristics, considering the knowledge is incomplete due to the environment and operational conditions. Here, at time t, the fuzzy measures denoted as $f(P_W(t))$ and $f(P_S(t))$ are derived from the Cauchy distribution by studying the expected value related to the forecasting value and materialized value, which is expressed as

$$f(P_W(t)) = \begin{cases} \dfrac{1}{1+\omega(\Delta P_W(t)/Q_W(t)^+)^2}, & \Delta P_W(t) > 0 \\ \dfrac{1}{1+\omega(\Delta P_W(t)/(1-Q_W(t)^-))^2}, & \text{otherwise} \end{cases} \tag{14}$$

$$f(P_S(t)) = \begin{cases} \dfrac{1}{1+\omega(\Delta P_S(t)/Q_S(t)^+)^2}, & \Delta P_S(t) > 0 \\ \dfrac{1}{1+\omega(\Delta P_S(t)/(1-Q_S(t)^-))^2}, & \text{otherwise} \end{cases} \tag{15}$$

where ω represents a weighting factor, and $\Delta P_W(t) = P_W(t) - \mu_W(t)$, $\Delta P_S(t) = P_S(t) - \mu_S(t)$.

The credibility function shown by (16), which is defined as the average of possibility and necessity measures [42], has been shown to satisfy the properties of dual, normality, monotonicity, and nonnegativity [28,43]. Taking uncertain wind power for example, based on credibility function, the credibility measure developed by (17) is applied to evaluate uncertain wind power, considering the random measure and fuzzy measure.

$$\mathrm{Cr}\{\xi \in A\} = \frac{1}{2}\left(\sup_{x(t)\in A} f(x(t)) + 1 - \sup_{x(t)\in A^c} f(x(t))\right) \tag{16}$$

$$\begin{aligned} \nu(P_W(t)) &= \mathrm{Cr}\{\xi \le \Delta P_W(t)\} \\ &= \begin{cases} 1 - \dfrac{1}{2[1+\omega(\Delta P_W(t)/Q_W(t)^+)^2]}, & \Delta P_W(t) > 0 \\ \dfrac{1}{2[1+\omega(\Delta P_W(t)/(1-Q_W(t)^-)^2)]}, & \Delta P_W(t) \le 0 \end{cases} \end{aligned} \tag{17}$$

where A represents a nonempty set, and $\nu(P_W(t))$ denotes the credibility measure associated with uncertain wind power.

Proof. According to (16), at time t, for $\Delta P_W(t) \in \Re$, we have

$$\mathrm{Cr}(\Delta P_W(t)) = \frac{1}{2}\left(1 + \sup_{y\le\Delta P_W(t)} f(y) - \sup_{y>\Delta P_W(t)} f(y)\right) \tag{18}$$

If $\Delta P_W(t) > 0$, we have

$$\begin{aligned} \sup_{y\le\Delta P_W(t)} f(y) &= \max\left\{\sup_{0<y\le\Delta P(t)} f(y),\ \sup_{y\le 0} f(y)\right\} \\ &= \max\{f(0), f(0)\} \\ &= 1 \end{aligned} \tag{19}$$

and

$$\begin{aligned}\sup_{y>\Delta P_{\mathrm{W}}(t)} f(y) &= \sup_{y>\Delta P_{\mathrm{W}}(t)>0} \frac{1}{1+\omega(y/Q_{\mathrm{W}}(t)^{+})^2} \\ &= \frac{1}{1+\omega(\Delta P_{\mathrm{W}}(t)/Q_{\mathrm{W}}(t)^{+})^2}\end{aligned} \tag{20}$$

Based on (19) and (20), the credibility measure is

$$\mathrm{Cr}(\Delta P_{\mathrm{W}}(t)) = 1 - \frac{1}{2[1+\omega(\Delta P_{\mathrm{W}}(t)/Q_{\mathrm{W}}(t)^{+})^2]}, \quad \Delta P_{\mathrm{W}}(t) > 0 \tag{21}$$

If $\Delta P_{\mathrm{W}}(t) \leq 0$, we have

$$\begin{aligned}\sup_{y\leq\Delta P_{\mathrm{W}}(t)} f(y) &= \sup_{y\leq\Delta P_{\mathrm{W}}(t)\leq 0} \frac{1}{1+\omega(y/(1-Q_{\mathrm{W}}(t)^{-})^2)} \\ &= \frac{1}{1+\omega(\Delta P_{\mathrm{W}}(t)/(1-Q_{\mathrm{W}}(t)^{-})^2)}\end{aligned} \tag{22}$$

and

$$\begin{aligned}\sup_{y>\Delta P_{\mathrm{W}}(t)} f(y) &= \max\left\{\sup_{y\leq\Delta P_{\mathrm{W}}(t)\leq 0} f(y), \sup_{y>0} f(y)\right\} \\ &= \max\left\{\sup_{\Delta P_{\mathrm{W}}(t)<y\leq 0} \frac{1}{1+\omega(y/(1-Q_{\mathrm{W}}(t)^{-})^2)}, \sup_{y>0} \frac{1}{1+\omega(y/Q_{\mathrm{W}}(t)^{-})^2}\right\} \\ &= f(0) \\ &= 1\end{aligned} \tag{23}$$

Based on (22) and (23), the credibility measure is

$$\mathrm{Cr}(\Delta P_{\mathrm{W}}(t)) = \frac{1}{2[1+\omega(\Delta P_{\mathrm{W}}(t)/(1-Q_{\mathrm{W}}(t)^{-})^2)]}, \quad \Delta P_{\mathrm{W}}(t) \leq 0 \tag{24}$$

This completes the proof. □

3.2. Load Partition Method

Define $\mu_{\mathrm{RE}}(t) = \mu_{\mathrm{W}}(t) + \mu_{\mathrm{S}}(t)$, and set $m_1 = \min\{P_{\mathrm{L0}}(t) - \mu_{\mathrm{RE}}(t)\}$, $m_2 = \mathrm{median}\{P_{\mathrm{L0}}(t) - \mu_{\mathrm{RE}}(t)\}$, and $m_3 = \max\{P_{\mathrm{L0}}(t) - \mu_{\mathrm{RE}}(t)\}$, $m_1 < m_2 < m_3$, $P_{\mathrm{L0}}(t)$ represents the initial load demand during time t. Based on the shortest distance method, the net load curve of WSTHcMEEM considering wind and solar power integration can be partitioned into peak period, flat period, and valley period using (25)–(27):

$$t \in G_1, \text{if } |P_{\mathrm{L0}}(t) - \mu_{\mathrm{RE}}(t) - m_1| = \min\{|P_{\mathrm{L0}}(t) - \mu_{\mathrm{RE}}(t) - m_j|_{j=1,2,3}\} \tag{25}$$

$$t \in G_2, \text{if } |P_{\mathrm{L0}}(t) - \mu_{\mathrm{RE}}(t) - m_2| = \min\{|P_{\mathrm{L0}}(t) - \mu_{\mathrm{RE}}(t) - m_j|_{j=1,2,3}\} \tag{26}$$

$$t \in G_3, \text{if } |P_{\mathrm{L0}}(t) - \mu_{\mathrm{RE}}(t) - m_3| = \min\{|P_{\mathrm{L0}}(t) - \mu_{\mathrm{RE}}(t) - m_j|_{j=1,2,3}\} \tag{27}$$

The main steps of load partition method are given as follows:

Step 1: Set $t = 1$. According to the forecasted load, and forecasted outputs of wind and solar power, rank $\{P_{\mathrm{L0}}(t) - \mu_{\mathrm{RE}}(t)\}$, and we have $P_1 < P_2 < \cdots < P_T \in \{P_{\mathrm{L0}}(t) - \mu_{\mathrm{RE}}(t))\}$. Then, obtain m_1, m_2, m_3.

Step 2: If $P_{\mathrm{L0}}(t) - \mu_{\mathrm{RE}}(t) \in [m_1, m_2]$, based on (25) and (26), we can obtain sets G_1 and G_2, respectively, i.e., $P_{\mathrm{L0}}(t) - \mu_{\mathrm{RE}}(t) - m_1 < m_2 - P_{\mathrm{L0}}(t) + \mu_{\mathrm{RE}}(t)$, $P_{\mathrm{L0}}(t) - \mu_{\mathrm{RE}}(t) \in G_1$; otherwise, $P_{\mathrm{L0}}(t) - \mu_{\mathrm{RE}}(t) \in G_2$.

Step 3: If $P_{\mathrm{L0}}(t) - \mu_{\mathrm{RE}}(t) \in [m_2, m_3]$, based on (26) and (27), we can determine sets G_2 and G_3, respectively, i.e., $P_{\mathrm{L0}}(t) - \mu_{\mathrm{RE}}(t) - m_2 < m_3 - P_{\mathrm{L0}}(t) + \mu_{\mathrm{RE}}(t)$, $P_{\mathrm{L0}}(t) - \mu_{\mathrm{RE}}(t) \in G_2$; otherwise, $P_{\mathrm{L0}}(t) - \mu_{\mathrm{RE}}(t) \in G_3$.

Step 4: $t = t + 1$. Continue 2 to 4 until $t > T$.

By (25)–(27), the demand sensitivity E can be written by:

$$E(t,t') = \frac{\rho_0(t')}{(P_{L0}(t) - \mu_{RE}(t))} \frac{\partial(P_D(t) - \mu_{RE}(t))}{\partial\rho(t')} \begin{cases} E(t,t') \leq 0 \text{ if } t = t' \\ E(t,t') \geq 0 \text{ if } t \neq t' \end{cases} \quad (28)$$

where $P_D(t)$ is the load demand after implementing DR during time t.

Therefore, according to E and the TOU price, the load demand with DR can be written by (29). Note that the participation percentage of load in DR is considered to be 20%.

$$P_D(t) = P_{L0}(t) \times \left(1 + \sum_{t'=1, t' \neq t}^{T} E(t,t') \frac{\rho(t') - \rho_0(t')}{\rho_0(t')}\right) \quad (29)$$

4. Simulation Studies

We consider the WSTHcMSSM system with one micro-turbine, one pumped hydro storage with two reservoirs, one wind turbine, and one solar turbine. The entire scheduling period is 24 h, and thus the installed capacities of wind, solar, micro-turbine, and hydro storage are fixed in this paper. In pumped hydro storage, two-chain cascade hydro turbines are considered on one stream to represent the complex hydro network. This subsection describes the main features of the operation characteristics of micro-turbine, pumped hydro storage, wind, and solar turbine under study. The hourly load demand, forecasted wind, and solar power are illustrated by Figure 2, and the standard deviations of wind and solar power outputs are set to 5% of the forecasted values.

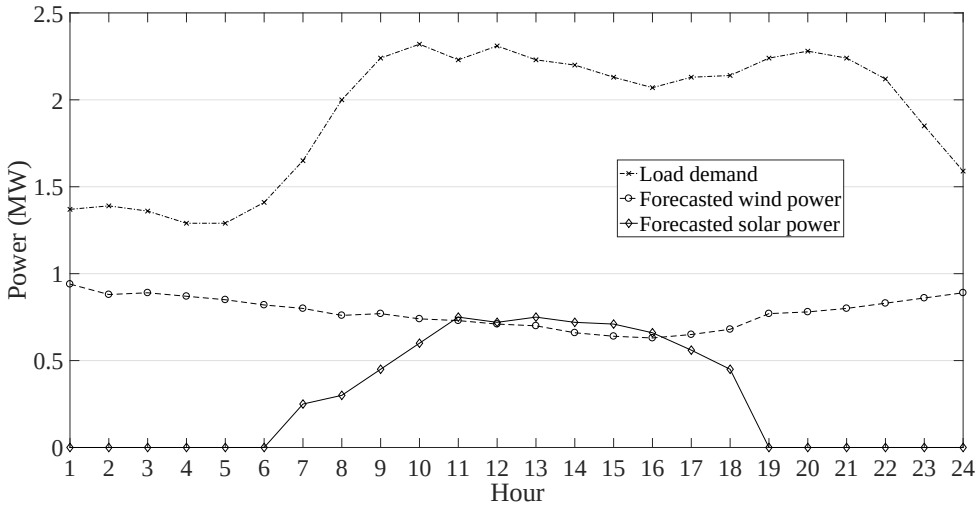

Figure 2. Hourly load demand, forecasted wind, and solar power.

In this paper, the optimization algorithm proposed in [44] is employed to solve the proposed model. The algorithm is inspired by studying the behavior of group animal searching and living theory. The practicability and feasibility of the algorithm have been proved in optimizing multi-modal engineering problems and benchmarks. For a detailed description of the algorithm, please refer to [44].

The initial electricity price is 220 $/MW. The maximum outputs of wind and solar unit are, respectively, 1.0 MW and 0.8 MW. The cost coefficients of the micro-turbine are $a_{1g} = 0.002$, $a_{2g} = 19.2$, $a_{3g} = 150$, and the operation limits of the micro-turbine are set to 0 MW and 0.8 MW. The ramp rate of the thermal unit is set to 0.55 MW. The initial and final reservoir storage volumes of the two reservoirs are, respectively, 1.0×10^4 m^3, 1.2×10^4 m^3, and 1.2×10^4 m^3, 1.4×10^4 m^3. The minimum volume values of the two reservoirs are, respectively, 0.8×10^4 m^3 and 0.7×10^4 m^3, and the maximum volume values of the two reservoirs are, respectively, 1.5×10^4 m^3 and 1.6×10^4 m^3. The pumped

hydro storage ranges from 0 MW to 0.6 MW, and the lower and upper boundaries of the water release are, respectively, 1×10^3 m^3 and 8×10^3 m^3. The generation coefficients of hydro units are $b_{11} = -0.0042, b_{21} - 0.42, b_{31} = 0.030, b_{41} = 0.90, b_{51} = 2.0, b_{61} = -2.0$, $b_{12} = -0.0040, b_{22} = -0.30, b_{32} = 0.015, b_{42} = 1.14, b_{52} = 2.5, b_{62} = -3$. The water transport delay time from reservoir 1 to reservoir 2 is set to 1 h. Suppose the spillage discharge rate of the reservoir is zero, and the external inflow to the reservoir at each time is given by Table 1.

Table 1. The hourly inflow to the reservoir (10^4 m^3).

Hour	1	2	3	4	5	6	7	8	9	10	11	12
Reservoir 1	0.60	0.54	0.48	0.42	0.36	0.42	0.48	0.54	0.60	0.66	0.72	0.60
Reservoir 2	0.48	0.48	0.54	0.54	0.48	0.42	0.36	0.42	0.48	0.54	0.54	0.48
Hour	13	14	15	16	17	18	19	20	21	22	23	24
Reservoir 1	0.66	0.72	0.66	0.60	0.54	0.48	0.42	0.36	0.42	0.48	0.54	0.60
Reservoir 2	0.48	0.54	0.54	0.48	0.42	0.36	0.42	0.48	0.54	0.54	0.48	0.48

Table 2 gives the optimal wind power, solar power, water discharge, TOU price, and load demand with DR over 30 independent runs. From the table, we can find that the optimal outputs meet the operation constraints. In addition, the reservoir volumes of the two reservoirs are illustrated by Figure 3. From the figure, we can see that the reservoir volumes are within their requirements. Moreover, note that the optimal wind and solar outputs are not their upper bounds. This is because the fact that a large penetration of renewable energy does not correspond to a large credibility measure. Figure 4 provides the distribution characteristics of credibility measure, operation profit, and wind and solar outputs. The correlation coefficient between credibility and wind and solar power is -0.0852, which means that these two aspects show a negative, but not significant, relationship. Additionally, we find that the correlation coefficient between profit and renewable energy is -0.0074. This phenomenon shows that a large penetration of renewable energy is not always a benefit for WSTHcMSSM considering the risk brought by uncertainty. On the other hand, we can conclude that the proposed CVaC-based quantitative risk evaluation method can make the WSTHcMSSM system a trade-off solution considering the uncertainty of wind and solar power.

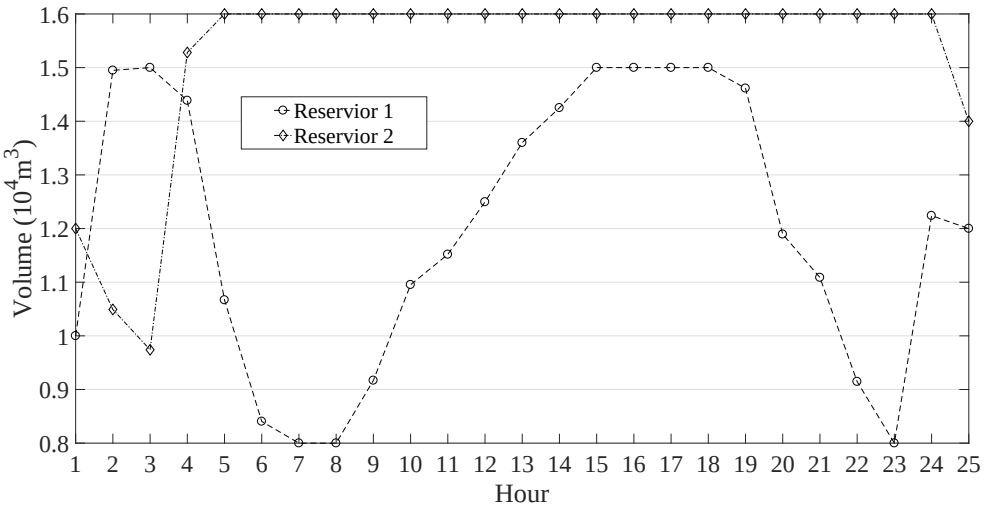

Figure 3. The reservoir volumes of the pumped hydro units.

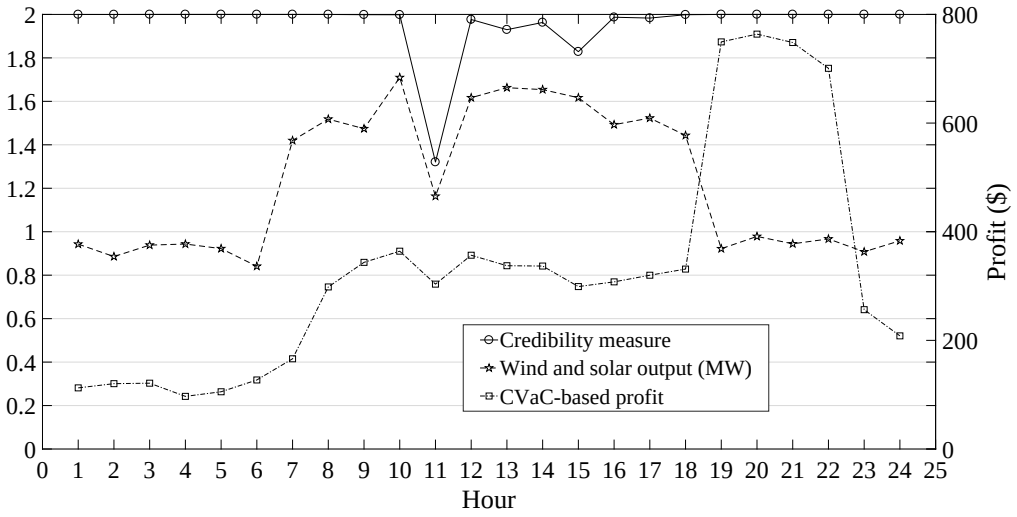

Figure 4. The characteristics of credibility measure, profit, and wind and solar power based on CVaC.

Table 2. Optimal water discharge, power outputs, TOU price, and load demand with DR.

Hour	Water Discharges (10^4 m^3)		Hydro Power (MW)		Wind (MW)	Solar (MW)	Thermal (MW)	TOU Price ($/MW)	Load with DR (MW)
	Unit 1	Unit 2	Unit 1	Unit 2					
1	0.1051	0.6309	0	0	0.9429	0	0.4733	191.84	1.4103
2	0.5312	0.6602	0.2493	0	0.8856	0	0.3019	191.41	1.4309
3	0.4723	0.5171	0.1607	0.0117	0.9384	0	0.2951	195.60	1.4000
4	0.3663	0.5032	0.0297	0.0079	0.9434	0	0.3526	186.33	1.3279
5	0.5863	0.4395	0.2286	0	0.9223	0	0.1827	197.44	1.3279
6	0.4683	0.6938	0	0.4119	0.8411	0	0.2046	192.69	1.4514
7	0.3990	0.4040	0	0	0.9230	0.4967	0.2860	188.55	1.6985
8	0.4231	0.5200	0.0477	0.0361	0.8507	0.6675	0.4568	220	2.0588
9	0.4216	0.5593	0.0918	0.1226	0.8382	0.6360	0.6173	220	2.3058
10	0.6036	0.3966	0.4866	0	0.9618	0.7477	0.1920	220	2.3882
11	0.6222	0.6222	0.5536	0.2506	0.9022	0.2611	0.3281	220	2.2955
12	0.4205	0.3718	0.1262	0	0.8445	0.7723	0.6349	220	2.3779
13	0.5259	0.3468	0.2999	0	0.8857	0.7771	0.3328	220	2.2955
14	0.4758	0.5579	0.3301	0.1109	0.8924	0.7616	0.1696	220	2.2647
15	0.5106	0.4725	0.2752	0	0.8860	0.7307	0.3007	220	2.1926
16	0.4473	0.3602	0.3937	0	0.7341	0.7585	0.2445	220	2.1308
17	0.4304	0.4304	0.1429	0	0.8855	0.6376	0.5266	220	2.1926
18	0.5185	0.6605	0.2532	0.3414	0.7890	0.6543	0.1650	220	2.2029
19	0.6921	0.7284	0.2722	0.4930	0.9219	0	0.3902	436.60	2.3058
20	0.4407	0.7635	0	0.5575	0.9783	0	0.5786	437.40	2.3470
21	0.6140	0.7649	0	0.5604	0.9444	0	0.5725	437.65	2.3058
22	0.6758	0.7167	0.0215	0.4685	0.9668	0	0.5092	437.94	2.1823
23	0.1160	0.6674	0	0.3561	0.9077	0	0.6406	220	1.9044
24	0.5550	0.8000	0.1809	0.4047	0.9584	0	0.0927	220	1.6367

The load curves with and without DR and pumped hydro storage are depicted by Figure 5. In Figure 5, the load characteristics with DR are much more smooth than these without considering DR. In order to show the load characteristics more intuitively, some factors used in [13] are employed, and these factors are given by Table 3. From the table, we can clearly see that DR is benefit for improving load curve. Specifically, compared with the load characteristics without DR, the load factors considering DR increase 3.01% and 5.50%, the peak to valley factors decrease 3.36% and 4.69%, and the peak compensate factors decrease 2.69% and 2.92%. On the other hand, the proposed WSTHcMSSM can explore

the potional flexibility in multi-resource complementarity for promoting the penetration of renewable energy.

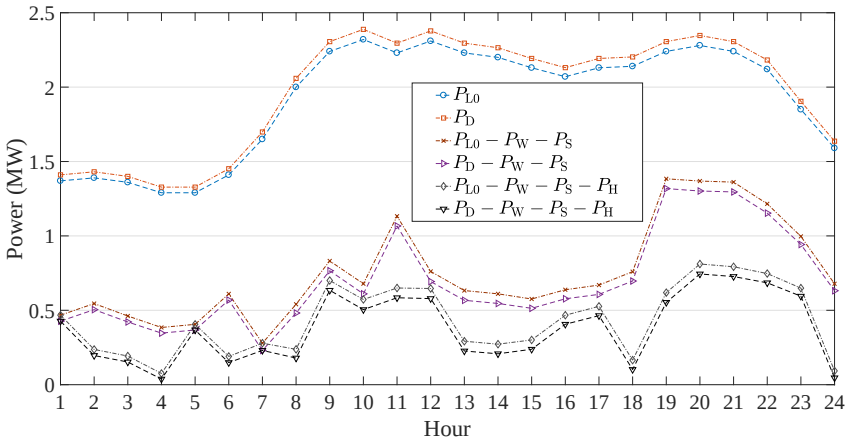

Figure 5. The load characteristics considering DR and pumped hydro storage.

Table 3. The comparison of load characteristics.

Factor	*Load-Factor* %	*Peak-to-Valley* %	*Peak-Compensate* %
$P_{L0} - P_W - P_S$	52.58	82.53	43.18
$P_D - P_W - P_S$	**54.16**	**79.85**	**42.05**
$P_{L0} - P_W - P_S - P_H$	50.58	94.93	67.96
$P_D - P_W - P_S - P_H$	**53.36**	**90.68**	**66.03**

Moreover, to validate the coupling characteristic of the uncertainty, the hourly wind, solar, and operation profit of WSTHcMSSM are given by Table 4. Considering the coupling characteristic of multiple sources uncertainty, the penetration levels of wind and solar power have increased 1.58% and 9.33%, respectively. The operation profit considering coupling characteristic has increased 63.6362$. The comparison illustrates that in WSTHcMSSM scheduling, the coupling of uncertain wind and solar power can mitigate the impact of uncertainty on system operation, and in future research, the virtual aggregation mechanism should be considered in WSTHcMSSM for addressing the uncertain renewable energy.

Additionally, the comparison results between the proposed CVaC model and interval optimization (IO) model [14,45] are shown in Table 5, where P_{WS} denotes the total outputs of wind and solar power. It can be observed from the obtained results that the proposed model performs better than IO model in terms of the profit and renewable energy penetration, which increases 13.8352% and 6.0152%, respectively. Note that a lower penetration level of renewable energy does not mean a lower level of risk. From the above analysis, it can be concluded that the proposed CVaC is more suitable than IO to provide a reliable guidance for WSTHcMSSM in day-ahead perspective, because it provides a flexible framework in realizing profit–risk trade-off and presents a reliable viewpoint for the dispatcher in choosing the best strategy for the optimal operation of WSTHcMSSM.

Furthermore, the optimal results obtained by CVaC considering different forecasting errors are illustrated in Figure 6. From the figure, we can find that a larger forecasting error corresponds to a lower penetration level of uncertain renewable energy and a smaller operation profit. This demonstrates that a larger forecasting error brings a higher operation risk, and thus the penetration level of uncertain renewable energy should be limited in WSTHcMSSM scheduling. Therefore, the proposed CVaC-based risk evaluation method can effectively address uncertain renewable energy in WSTHcMSSM scheduling. Specifically, for every 5% increase in forecasting error, the output of wind is reduced by the maximum of 0.73 MW, and the output of solar is reduced by the maximum of 0.24 MW, and the operation profit is reduced by the maximum of 759 $.

Table 4. Comparison results between CVaC with and without wind/solar coupling.

Hour	Wind and Solar Coupling-Based CVaC					Wind and Solar Independent-Based CVaC				
	P_W(MW)	$v(P_W)$	P_S(MW)	$v(P_S)$	H(\$)	P_W(MW)	$v(P_W)$	P_S(MW)	$v(P_S)$	H(\$)
1	0.9429	0.9998	0	1	112.56	0.9380	0.5000	0	1	20.24
2	0.8856	0.9997	0	1	120.31	0.9442	1	0	1	126.96
3	0.9384	1	0	1	120.09	0.8907	0.9754	0	1	104.30
4	0.9434	1	0	1	93.85	0.9200	1	0	1	104.02
5	0.9223	1	0	1	111.81	0.8930	1	0	1	103.05
6	0.8411	1	0	1	127.57	0.8580	1	0	1	131.57
7	0.9230	1	0.4967	1	166.11	0.9310	1	0.1948	0.5000	157.94
8	0.8507	0.9999	0.6675	1	299.24	0.8360	1	0.5384	0.9946	293.46
9	0.8382	0.9988	0.6360	0.9999	350.69	0.7959	1	0.5913	0.9945	348.88
10	0.9618	1	0.7477	0.9985	371.71	0.7825	1	0.6183	0.9931	369.99
11	0.9022	0.9999	0.2611	0.3207	312.87	0.8500	1	0.7504	0.9767	345.83
12	0.8445	0.9993	0.7723	0.9786	357.19	0.7564	1	0.7551	1	371.30
13	0.8857	0.9999	0.7771	0.9314	337.06	0.9096	1	0.7517	1	343.39
14	0.8924	1	0.7616	0.9628	339.40	0.8006	1	0.2765	0.3994	304.08
15	0.8860	1	0.7307	0.8289	300.46	0.8250	1	0.7200	1	327.19
16	0.7341	0.9934	0.7585	0.9937	312.77	0.7326	1	0.6913	1	311.22
17	0.8855	1	0.6376	0.9829	319.86	0.8237	1	0.6930	1	325.20
18	0.7890	0.9987	0.6543	1	333.71	0.7862	1	0.6463	1	330.84
19	0.9219	1	0	1	750.50	0.9904	1	0	1	751.51
20	0.9783	1	0	1	764.13	0.9922	1	0	1	769.13
21	0.9444	1	0	1	748.63	0.9822	1	0	1	741.69
22	0.9668	1	0	1	700.81	0.9730	1	0	1	703.19
23	0.9077	1	0	1	257.72	0.9975	1	0	1	259.33
24	0.9584	1	0	1	207.89	0.9998	1	0	1	209.01
Total	**21.5442**		**7.9011**		**7916.96**	21.2083		7.2268		7853.32

Table 5. Comparison results between CVaC and IO model.

Hour	The Proposed Model					Interval Optimization Model				
	$v(P_W)$	$v(P_S)$	H(\$)	P_{WS}(MW)	P_H(MW)	$v(P_W)$	$v(P_S)$	H(\$)	P_{WS}(MW)	P_H(MW)
1	0.9998	1	112.56	0.9429	0	0.4982	1	26.63	0.9096	0
2	0.9997	1	120.31	0.8856	0.2493	0.4891	1	46.01	0.8012	0.3547
3	1	1	120.09	0.9384	0.1724	0.4738	1	40.26	0.7598	0.2952
4	1	1	93.85	0.9434	0.0376	0.4966	1	20.76	0.8280	0.1525
5	1	1	111.81	0.9223	0.2286	0.4542	1	36.14	0.6659	0.5102
6	1	1	127.57	0.8411	0.4119	0.4972	1	56.02	0.7826	0.5638
7	1	1	166.11	1.4197	0	1	1	179.69	1.3124	0.0275
8	0.9999	1	299.24	1.5182	0.0838	1	1	300.20	1.4550	0.4554
9	0.9988	0.9999	350.69	1.4742	0.2144	0.9996	0.9989	347.48	1.4397	0.3609
10	1	0.9985	371.71	1.7096	0.4866	0.9984	0.4996	303.29	1.4137	0.5692
11	0.9999	0.3207	312.87	1.1633	0.8042	0.9759	0.4994	266.09	1.5070	0.5444
12	0.9993	0.9786	357.19	1.6167	0.1262	0.5217	0.4893	216.91	1.3389	0.4663
13	0.9999	0.9314	337.06	1.6628	0.2999	0.9632	0.4921	270.90	1.4185	0.6997
14	1	0.9628	339.40	1.6540	0.4411	0.9997	0.5000	267.69	1.5610	0.5968
15	1	0.8289	300.46	1.6166	0.2752	0.9875	0.9326	315.83	1.4726	0.5309
16	0.9934	0.9937	312.77	1.4927	0.3937	0.9984	0.4953	245.19	1.3723	0.3918
17	1	0.9829	319.86	1.5231	0.1429	0.9995	0.9932	326.39	1.4797	0.4511
18	0.9987	1	333.71	1.4433	0.5946	1	1	332.75	1.6073	0.4914
19	1	1	750.50	0.9219	0.7652	1	1	753.49	0.8920	0.7958
20	1	1	764.13	0.9783	0.5575	1	1	762.30	0.9952	0.5894
21	1	1	748.63	0.9444	0.5604	1	1	751.76	0.9930	0.5928
22	1	1	700.81	0.9668	0.4900	1	1	706.75	0.9939	0.6607
23	1	1	257.72	0.9077	0.3651	1	1	262.23	0.9893	0.5591
24	1	1	207.89	0.9584	0.5856	0.4822	1	120.01	0.7860	0.8187
Total			**7916.96**	**29.4453**	8.2775			6954.76	27.7746	**11.4783**

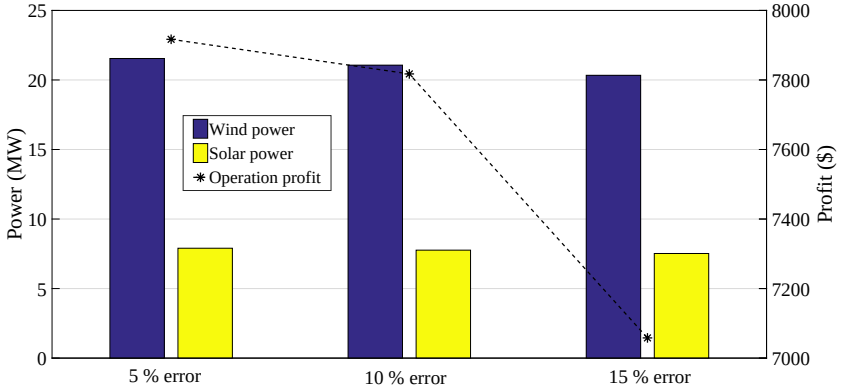

Figure 6. Optimal profit, wind, and solar power under different forecasting errors.

In order to further demonstrate the effectiveness of the proposed model for addressing the uncertain renewable energy, the stochastic model using (9) and the fuzzy model using (14) or (15) are employed for comparison. The credibility measures and profit values (H) obtained by different models are given by Table 6. From the table, we can see that the proposed model can obtain a high profit with a large credibility in most cases.

Table 6. Comparison of fuzzy model, stochastic model, and the proposed model.

	Fuzzy Model			Stochastic Model			Proposed Model		
Hour	$\nu(P_W)$	$\nu(P_S)$	**H($)**	$\nu(P_W)$	$\nu(P_S)$	**H($)**	$\nu(P_W)$	$\nu(P_S)$	**H($)**
1	0.4899	1	28.26	0.4317	1	28.97	0.9998	1	112.56
2	0.4888	1	41.37	0.4708	1	41.56	0.9997	1	120.31
3	0.4452	1	43.32	0.2397	1	78.86	1	1	120.09
4	0.4603	1	30.63	0.3356	1	38.17	1	1	93.85
5	0.4795	1	34.82	0.4243	1	23.53	1	1	111.81
6	0.4997	1	42.57	0.3199	1	75.08	1	1	127.57
7	0.4973	0.4939	84.20	0.2110	1	151.06	1	1	166.11
8	0.4999	0.5000	178.75	0.8967	1	270.23	0.9999	1	299.24
9	0.4995	0.4817	222.39	0.5000	0.8544	245.67	0.9988	0.9999	350.69
10	0.4999	0.4964	220.56	0.4481	0.4906	240.36	1	0.9985	371.71
11	0.4959	0.4673	199.54	0.4423	0.2832	249.54	0.9999	0.3207	312.87
12	0.4951	0.4931	218.02	0.2988	0.4878	263.45	0.9993	0.9786	357.19
13	0.4993	0.4777	201.09	0.9995	0.3888	286.75	0.9999	0.9314	337.06
14	0.5006	0.4673	201.73	0.9954	0.2818	313.45	1	0.9628	339.40
15	0.5000	0.4734	184.58	0.4001	0.3792	229.56	1	0.8289	300.46
16	0.4979	0.4864	183.43	1	0.3393	274.23	0.9934	0.9937	312.77
17	0.5160	0.5171	187.89	0.3450	0.9997	288.54	1	0.9829	319.86
18	0.5842	0.7767	233.08	0.3490	0.9973	284.79	0.9987	1	333.71
19	0.9998	1	748.64	1	1	740.04	1	1	750.50
20	0.4985	1	603.11	1	1	755.19	1	1	764.13
21	0.5000	1	566.89	0.4964	1	583.85	1	1	748.63
22	0.5000	1	521.25	0.4558	1	546.96	1	1	700.81
23	0.4990	1	166.40	0.4298	1	179.94	1	1	257.72
24	0.4508	1	123.04	0.1766	1	194.06	1	1	207.89
Total			5252.17			6383.83			**7916.96**

The hourly wind and solar power of each model are provided in Figure 7, and the total wind and solar power integrated with fuzzy model, stochastic model, and the proposed model are, respectively, 23.2275 MW, 17.9877 MW, and 29.4453 MW. The results show that compared with the proposed model, both the fuzzy and stochastic models are conservative in assessing uncertain renewable energy. Additionally, these results also illustrate that a higher wind or solar power output does not always correspond to a higher risk.

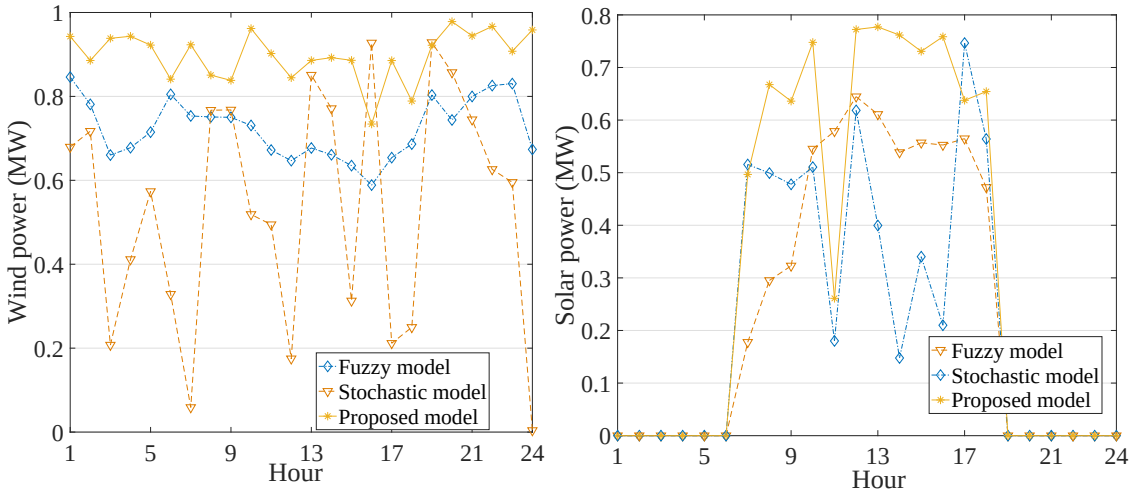

Figure 7. Optimal hourly output of wind and solar power under different models.

5. Conclusions

This paper developed a multi-source-coupled system applicable to standalone microgrid with pumped hydro storage and DR. The multi-source complementarity can efficiently explore the potential flexibility in WSTHcMSSM. Using the CVaC-based quantitative risk-averse model for uncertain wind and solar power makes this system a trade-off option. The designed load partitioning method takes into account the load characteristic, wind and solar distribution to get the TOU price in DR. The experimental test demonstrated that the WSTHcMSSM system can efficiently coordinate the outputs of thermal power, wind power, solar power, and pumped hydro storage to maximize operation profit. The simulation results show that the multi-source coordinating can increase operation profit, and promote wind and solar power accommodation. It found that DR plays an important role in smoothing the load curve of WSTHcMSSM system, in terms of increasing load factor, decreasing both peak compensate and peak to valley factors. The wind and solar coupling-based CVaC can increase 1.5838% and 9.3305% wind and solar power penetration levels, respectively.

The main challenge of the risk-averse model is that the forecasting error is modeled on the Gaussian distribution. The motivation for using this distribution is the central limit theorem. In future work, the proposed methodology can be extended for studying uncertain renewable energy in multi-energy and multiple microgrids scheduling and planning problems. In addition, future work could look at the distributed WSTHcMSSM system of the proposed framework in a reward fairness-based DR scheme with more than one distributed generation source. Future work could also focus on the economic and technical analysis on the sharing dispatchable source in distributed WSTHcMSSM.

Author Contributions: Conceptualization, methodology, and investigation: Y.Z., writing—review, editing and supervising, funding acquisition: J.C. All authors have read and agreed to the published version of the manuscript.

Funding: This work was supported by A Project of Shandong Province Higher Educational Science and Technology Program of China, under Grant number J18KA019.

Data Availability Statement: The data used to support the findings of this study are available from the corresponding author upon request.

Acknowledgments: This work was supported by A Project of Shandong Province Higher Educational Science and Technology Program of China under Grant (J18KA019).

Conflicts of Interest: The authors declare that there are no conflicts of the interest regarding the publication of this article.

References

1. Aleixandretudo, J.L.; Castellocogollos, L.; Aleixandre, J.L.; Aleixandrebenavent, R. Renewable energies: Worldwide trends in research, funding and international collaboration. *Renew. Energy* **2019**, *139*, 268–278. [CrossRef]
2. Yoshida, Y.; Farzaneh, H. Optimal design of a stand-alone residential hybrid Microgrid system for enhancing renewable energy deployment in Japan. *Energies* **2020**, *13*, 1737. [CrossRef]
3. Elmouatamid, A.; Ouladsine, R.; Bakhouya, M.; El Kamoun, N.; Khaidar, M.; Zine-Dine, K. Review of Control and Energy Management Approaches in Micro-Grid Systems. *Energies* **2021**, *14*, 168. [CrossRef]
4. Yang, X.; Xu, C.; Zhang, Y.; Yao, W.; Wen, J.; Cheng, S.J. Real-Time Coordinated Scheduling for ADNs with Soft Open Points and Charging Stations. *IEEE Trans. Power Syst.* **2021**, doi:10.1109/TPWRS.2021.3070036.
5. Ma, T.; Yang, H.; Lu, L. Feasibility study and economic analysis of pumped hydro storage and battery storage for a renewable energy powered island. *Energy Convers. Manag.* **2014**, *79*, 387–397. [CrossRef]
6. Liu, Y.; Shen, Z.; Tang, X.; Lian, H.; Li, J.; Gong, J. Worst-case conditional value-at-risk based bidding strategy for wind-hydro hybrid systems under probability distribution uncertainties. *Appl. Energy* **2019**, *256*, 113918. [CrossRef]
7. Liu, Y.; Ye, Y.; Chen, X.; Li, H.; Huang, Y. Robust Day-Ahead Dispatch for Integrated Power-Heat-Gas Microgrid considering Wind Power Uncertainty. *Math. Probl. Eng.* **2020**, *2020*, 1–12. [CrossRef]
8. Wang, X.; Chang, J.; Meng, X.; Wang, Y. Short-term hydro-thermal-wind-photovoltaic complementary operation of interconnected power systems. *Appl. Energy* **2018**, *229*, 945–962. [CrossRef]
9. Reddy, S.S. Optimal scheduling of thermal-wind-solar power system with storage. *Renew. Energy* **2017**, *101*, 1357–1368. [CrossRef]
10. Wang, Y.; Zhao, M.; Chang, J.; Wang, X.; Tian, Y. Study on the combined operation of a hydro-thermal-wind hybrid power system based on hydro-wind power compensating principles. *Energy Convers. Manag.* **2019**, *194*, 94–111. [CrossRef]

11. Zhang, D.; Du, T.; Yin, H.; Xia, S.; Zhang, H. Multi-Time-Scale Coordinated Operation of a Combined System with Wind-Solar-Thermal-Hydro Power and Battery Units. *Appl. Sci.* **2019**, *9*, 3574. [CrossRef]
12. Ross, M.; Abbey, C.; Bouffard, F.; Joos, G. Microgrid Economic Dispatch With Energy Storage Systems. *IEEE Trans. Smart Grid* **2018**, *9*, 3039–3047. [CrossRef]
13. Chen, J.J.; Qi, B.X.; Peng, K.; Li, Y.; Zhao, Y.L. Conditional value-at-credibility for random fuzzy wind power in demand response integrated multi-period economic emission dispatch. *Appl. Energy* **2020**, *261*, 114337. [CrossRef]
14. Chen, J.J.; Zhuang, Y.B.; Li, Y.Z.; Wang, P.; Zhao, Y.L.; Zhang, C.S. Risk-aware short term hydro-wind-thermal scheduling using a probability interval optimization model. *Appl. Energy* **2017**, *189*, 534–554. [CrossRef]
15. Jiao, P.; Chen, J.; Peng, K.; Zhao, Y.; Xin, K. Multi-objective mean-semi-entropy model for optimal standalone micro-grid planning with uncertain renewable energy resources. *Energy* **2019**, *191*, 116497. [CrossRef]
16. Huang, K.; Liu, P.; Ming, B.; Kim, J.S.; Gong, Y. Economic operation of a wind-solar-hydro complementary system considering risks of output shortage, power curtailment and spilled water. *Appl. Energy* **2021**, *290*, 116805. [CrossRef]
17. Menezes, R.F.A.; Soriano, G.D.; de Aquino, R.R.B. Locational Marginal Pricing and Daily Operation Scheduling of a Hydro-Thermal-Wind-Photovoltaic Power System Using BESS to Reduce Wind Power Curtailment. *Energies* **2021**, *14*, 1441. [CrossRef]
18. Pandey, M.; Winkler, D.; Sharma, R.; Lie, B. Using MPC to Balance Intermittent Wind and Solar Power with Hydro Power in Microgrids. *Energies* **2021**, *14*, 874. [CrossRef]
19. Hussain, A.; Kim, H.M. Goal-Programming-Based Multi-Objective Optimization in Off-Grid Microgrids. *Sustainability* **2020**, *12*, 8119. [CrossRef]
20. Yuan, H.; Xu, Y. Preventive-corrective coordinated transient stability dispatch of power systems with uncertain wind power. *IEEE Trans. Power Syst.* **2020**, *35*, 3616–3626. [CrossRef]
21. Chen, J.; Qi, B.; Rong, Z.; Peng, K.; Zhao, Y.; Zhang, X. Multi-energy coordinated microgrid scheduling with integrated demand response for flexibility improvement. *Energy* **2021**, *217*, 119387. [CrossRef]
22. Li, Y.; Wu, Q.H.; Li, M.S.; Zhan, J.P. Mean-variance model for power system economic dispatch with wind power integrated. *Energy* **2014**, *72*, 510–520. [CrossRef]
23. Joro, T.; Na, P. Portfolio performance evaluation in a mean-variance-skewness framework. *Eur. J. Oper. Res.* **2006**, *175*, 446–461. [CrossRef]
24. Chen, J.J.; Wu, Q.H.; Zhang, L.; Wu, P.Z. Multi-objective mean–variance–skewness model for nonconvex and stochastic optimal power flow considering wind power and load uncertainties. *Eur. J. Oper. Res.* **2017**, *263*, 719–732. [CrossRef]
25. Markowitz, H.M. *Portfolio Selection: Efficient Diversification of Investments*; John Wiley: Hoboken, NJ, USA, 1971.
26. Li, Y.; Wu, Q.H. Downside Risk Constrained Probabilistic Optimal Power Flow With Wind Power Integrated. *IEEE Trans. Power Syst.* **2016**, *31*, 1649–1650. [CrossRef]
27. Li, Y.Z.; Li, K.; Wang, P.; Liu, Y.; Lin, X.; Gooi, H.B.; Li, G.; Cai, D.; Luo, Y. Risk constrained economic dispatch with integration of wind power by multi-objective optimization approach. *Energy* **2017**, *126*, 810–820. [CrossRef]
28. Zhou, J.; Li, X.; Pedrycz, W. Mean-Semi-Entropy Models of Fuzzy Portfolio Selection. *IEEE Trans. Fuzzy Syst.* **2016**, *24*, 1627–1636. [CrossRef]
29. Feng, Y.; Wu, W.; Zhang, B.; Li, W. Power System Operation Risk Assessment Using Credibility Theory. *IEEE Trans. Power Syst.* **2008**, *23*, 1309–1318. [CrossRef]
30. Abdulrahman, K.H.; Shahidehpour, S.M. Static security in power system operation with fuzzy real load conditions. *IEEE Trans. Power Syst.* **1995**, *10*, 77–87. [CrossRef]
31. Unni, A.C.; Ongsakul, W.; Madhu, M.N. Fuzzy-based novel risk and reward definition applied for optimal generation-mix estimation. *Renew. Energy* **2020**, *148*, 665–673. [CrossRef]
32. Alawami, A.T.; Amleh, N.; Muqbel, A. Optimal Demand Response Bidding and Pricing Mechanism With Fuzzy Optimization: Application for a Virtual Power Plant. *IEEE Trans. Ind. Appl.* **2017**, *53*, 5051–5061. [CrossRef]
33. Gundogdu, F.K.; Kahraman, C. A novel spherical fuzzy analytic hierarchy process and its renewable energy application. *Soft Comput.* **2020**, *24*, 4607–4621. [CrossRef]
34. Simonelli, M.R. Indeterminacy in portfolio selection. *Eur. J. Oper. Res.* **2005**, *163*, 170–176. [CrossRef]
35. Silva, A.M.L.D.; Castro, J.F.C.; Gonzalezfernandez, R.A. Spinning Reserve Assessment Under Transmission Constraints Based on Cross-Entropy Method. *IEEE Trans. Power Syst.* **2016**, *31*, 1624–1632. [CrossRef]
36. Silva, A.M.L.D.; De Castro, A.M. Risk Assessment in Probabilistic Load Flow via Monte Carlo Simulation and Cross-Entropy Method. *IEEE Trans. Power Syst.* **2019**, *34*, 1193–1202. [CrossRef]
37. Moura, P.S.; De Almeida, A.T. The role of demand-side management in the grid integration of wind power. *Appl. Energy* **2010**, *87*, 2581–2588. [CrossRef]
38. Kirilenko, A.; Gong, Y.; Chung, C. A Framework for Power System Operational Planning under Uncertainty Using Coherent Risk Measures. *IEEE Trans. Power Syst.* **2021**,doi:10.1109/TPWRS.2021.3060427.
39. Behboodi, S.; Chassin, D.P.; Crawford, C.; Djilali, N. Renewable resources portfolio optimization in the presence of demand response. *Appl. Energy* **2016**, *162*, 139–148. [CrossRef]
40. Wang, Y.Q.; Zhou, J.Z.; Mo, L.; Zhang, R.; Zhang, Y.C. Short-term hydrothermal generation scheduling using differential real-coded quantum-inspired evolutionary algorithm. *Energy* **2012**, *44*, 657–671. [CrossRef]

41. Mandelbrot, B.B. The variation of certain speculative prices. In *Fractals and Scaling in Finance*; Springer: Berlin/Heidelberg, Germany, 1997; pp. 371–418.
42. Liu, B.; Liu, Y. Expected value of fuzzy variable and fuzzy expected value models. *IEEE Trans. Fuzzy Syst.* **2002**, *10*, 445–450.
43. Jiang, Z.; Wu, W.; Qin, H.; Zhou, J. Credibility theory based panoramic fuzzy risk analysis of hydropower station operation near the boundary. *J. Hydrol.* **2018**, *565*, 474–488. [CrossRef]
44. Chen, J.J.; Wu, Q.H.; Ji, T.Y.; Wu, P.; Li, M.S. Evolutionary predator and prey strategy for global optimization. *Inf. Sci.* **2016**, *327*, 217–232. [CrossRef]
45. Li, Y.Z.; Wu, Q.H.; Jiang, L.; Yang, J.B. Optimal Power System Dispatch With Wind Power Integrated Using Nonlinear Interval Optimization and Evidential Reasoning Approach. *IEEE Trans. Power Syst.* **2016**, *31*, 2246–2254. [CrossRef]